Molecular tagging velocimetry measurements of axial flow in a concentrated vortex core

Douglas G. Bohl
Naval Surface Warfare Center Indian Head Division, Indian Head, Maryland 20640

Manoochehr M. Koochesfahani
Michigan State University, East Lansing, Michigan 48824

(Received 21 April 2004; accepted 9 August 2004; published online 7 October 2004)

The characteristics of the axial flow within the core of a concentrated line vortex are investigated using molecular tagging velocimetry (MTV). A well-defined array of isolated vortices of alternating sign is generated in the wake of a NACA-0012 airfoil pitching sinusoidally at small amplitude and high reduced frequencies. The circulation and peak vorticity of the vortices are varied by the choice of oscillation frequency. Interaction of these two-dimensional vortices with the walls of the test section generates an axial flow within the vortex cores. The magnitude of the axial flow and its spatial/temporal characteristics are quantified using the MTV technique. Results show that the peak axial flow speeds can be very high, of the order maximum swirl speed of the vortices. The maximum axial speed ratio (maximum axial speed normalized by maximum swirl speed) is found to vary in the range 0.6–1.0 for the parameters investigated here. Initially, the axial flow is spatially confined in isolated structures corresponding to the core of vortices. As the vortex convects downstream, however, the spatial structure of axial flow changes from isolated regions to a continuous region for the highest reduced frequency investigated here. This change in structure is correlated with a significant decrease in the peak axial flow speed. © *2004 American Institute of Physics*.
[DOI: 10.1063/1.1802831]

I. INTRODUCTION

Flows with strong concentrated vortices are prevalent in many technological (e.g., wing-tip vortices, hydrocyclones) and natural (e.g., tornadoes, hurricanes, dust devils) flow fields. The interaction of vortices with other vortices, with boundaries (e.g., no-slip, free surface), with particles, etc., is a fundamental problem in fluid mechanics. In many vortical flows the presence of axial flow is an important feature of the vortex structure. It is well known that the interaction of a vortex with a no-slip boundary is one mechanism that causes a flow to be initiated along the axis of the vortex. A specific example where a vortex no-slip interaction is of interest is in the passage of helicopter rotor blades. Vortex blade interaction, in which the trailing vortex from a blade interacts with a following blade, is a major source of helicopter noise. Understanding and reducing the effects of the interaction is critical in reducing the noise signature.[1] In this work the interaction of concentrated vortices with a no-slip boundary condition and the subsequent structure of the axial core flow was investigated using molecular tagging velocimetry (MTV).

Initial work in the area of rotational flow near a no-slip boundary, including the start-up axial flow within a vortex core, and the resulting three-dimensional (3D) core structure can be found in von Kármán,[2] Bödewadt,[3] Rott and Lewellen,[4] and Burggraf *et al.*[5] In a study of vortex shedding behind an oscillating NACA-0012 airfoil, Koochesfahani[6] observed that axial flow developed within the isolated vortex cores due to the interaction with solid no-slip boundaries (i.e., the tunnel side walls and/or false walls placed in the flow). Using dye flow visualization, the magnitude of axial flow speed was estimated from the displacement of dye and appeared to vary linearly (for constant oscillation amplitude) with the reduced frequency. The magnitude was found to be significant with respect to the freestream velocity (in the range 30%–65% of freestream speed). In a similar geometry, Cohn and Koochesfahani[7] used flow visualization to look at the boundary conditions that initiate axial flow. It was found that axial flow was initiated for the no-slip boundary, as expected. However, axial flow was also initiated for a shear boundary condition. The core structure was different visually between the two cases. Specifically, the solid wall boundary created a core structure with the highest axial flow near the center of the vortex core (i.e., "single-cell" structure). In contrast, the shear boundary created a core axial velocity profile that indicated a maximum velocity near the edge of the vortex with a smaller axial velocity near the center (i.e., "multicell" structure). Hagen and Kurosaka[8] used heated fluid as a passive tracer in a hairpin vortex created by a ramp protruding into a flow. The results confirmed the corewise transport of the heated fluid within the vortex core with a velocity of the same order as the freestream velocity.

Laursen *et al.*[9] performed particle image velocimetry (PIV) measurements and dye visualization on a 2D line vortex pair created by ejecting fluid through a slit, traveling in a still fluid. It was observed that the initially 2D vortex quickly became unstable and broke up. Evidence for the breakup indicated that axial flow within the vortex core was responsible. Hirsa *et al.*[10] investigated the evolution of a columnar vortex with a no-slip boundary for early times near a bound-

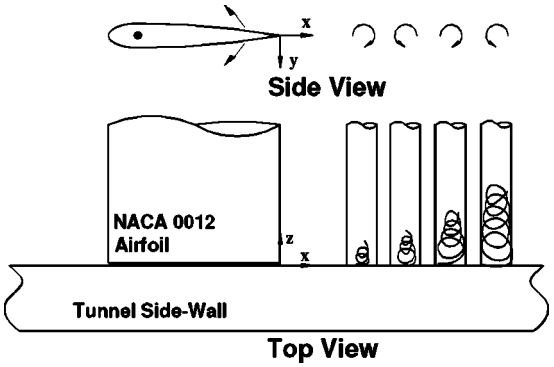

FIG. 1. Schematic representation of vortex/side-wall interaction.

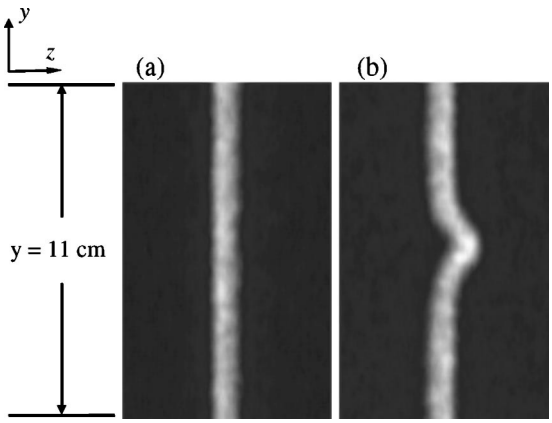

FIG. 2. Sample images of (a) the initial tagging pattern and (b) the same tagged region 17 ms later. Images show axial motion within the core of a concentrated vortex.

ary. It was shown, using a combination of experimental and computational methods, that the vortex structure developed a recirculation region (in the axial/radial plane) within the vortex core near the boundary. This recirculation region was attributed to the spatially oscillatory boundary layer structure associated with Bödewadt-type flows.

There is generally limited quantitative experimental data available on the actual magnitude and spatial structure of the axial flow within the core of a well-characterized concentrated vortex that is in contact with a solid wall. This type of data is helpful to the understanding of vortex–wall interactions and the nature of vortex core three dimensionality. The work described here considers the flow geometry previously investigated by Koochesfahani,[6] i.e., the axial flow within the vortex array created in the wake of an oscillating airfoil. The appeal in using this geometry resides in the fact that a well-defined isolated vortex array can be generated and their interactions with a solid wall can be systematically investigated. Previously, in this flow only qualitative information about axial flow has been available based on passive tracer flow visualization. The purpose of the current work was to quantitatively measure the axial flow characteristics and correlate them with the properties of the vortex.

II. EXPERIMENTAL SETUP

The experiments were conducted in a 10 000 L water tunnel (ELD, Inc.) with a 61 cm$\times$61 cm$\times$243 cm test section. A NACA-0012 airfoil with chordlength $C=12$ cm was placed in a freestream velocity $U_\infty=10.5$ cm/s, resulting in a chord Reynolds number $Re_c=12\,600$. This Reynolds number was chosen to closely match the conditions reported in Koochesfahani[6] and Cohn and Koochesfahani.[7] The airfoil oscillated sinusoidally about its 1/4-C axis with an amplitude of 2° and a frequency f in the range 1.18–3.21 Hz. This corresponded to a variation of the reduced frequency $k=(2\pi fC)/2U_\infty$ in the range 4.2–11.5. The reduced frequency served as the control parameter and allowed the vortex properties such as circulation and peak vorticity to be varied. The well-defined array of concentrated vortices that were shed from the trailing edge of the oscillating airfoil interacted with the side walls of the flow facility, resulting in an axial flow along the cores of the vortices. A schematic of the flow geometry is shown in Fig. 1.

The measurements were made using MTV. MTV is an optical technique that relies on molecules that can be turned into long lifetime tracers upon excitation by photons of an appropriate wavelength. Typically a pulsed laser is used to "tag" the regions of interest, and those tagged regions are interrogated at two successive times within the lifetime of the tracer. The measured Lagrangian displacement of the tagged regions provides the estimate of the fluid velocity vector. One might think of MTV as a *molecular* counterpart of PIV. In this work, water-soluble phosphorescent molecules were used along with an excimer laser providing 20 ns pulses at a wavelength of 308 nm. Details of this experimental technique can be found in Gendrich *et al.*[11] and Koochesfahani.[12]

Information on the axial velocity profile was obtained using a line tagging approach. In this work the laser line was passed vertically into the test section (i.e., normal to the bottom surface of the tunnel, along the y axis) and imaged from the downstream end of the tunnel (i.e., the y-z plane). In this orientation, motion in the z direction could be measured. Details of the experimental setup can be found in Bohl.[13] An example of such a molecularly tagged line at the time of laser firing is depicted in Fig. 2(a). In this figure the streamwise flow is out of the page and the vortex axis is in the z direction. The tagged line shown passes through the center of a passing vortex core. The z-direction displacement of the tagged line shown in Fig. 2(b) reveals a well-defined single-cell axial flow pattern within the vortex core. The measured displacement of the tagged line provides the quantitative estimate of the profile of the velocity component perpendicular to the line. Line displacement was determined for each row by finding the location of the line center in the delayed image relative to that in the initially tagged (i.e., undelayed) image. This was done by finding first the peak intensity along an image row (i.e., normal to the tagged line) to the nearest pixel. Subpixel accuracy was achieved by fitting the line intensity profile near the peak location to a polynomial, typically second order, see Fig. 3(a). Applying this procedure to the image pair in Fig. 2 results in the axial velocity profile $w(y)$ across the vortex core, illustrated in Fig. 3(b).

There are two sources of error in the line-tagging mea-

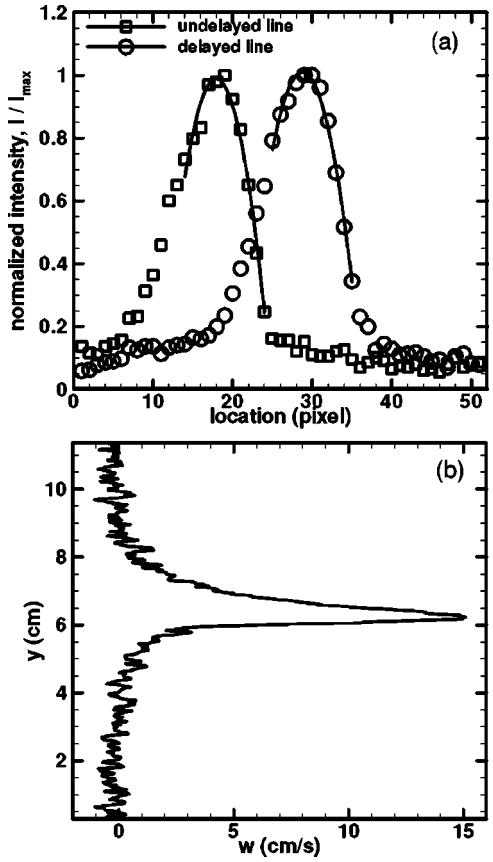

FIG. 3. (a) Sample intensity profiles taken from Fig. 2 in the region of line displacement. Solid lines shown are the best fit of second order polynomial to ±5 data points about the peak intensity location. (b) Resulting velocity profile along the tagged line in Fig. 2.

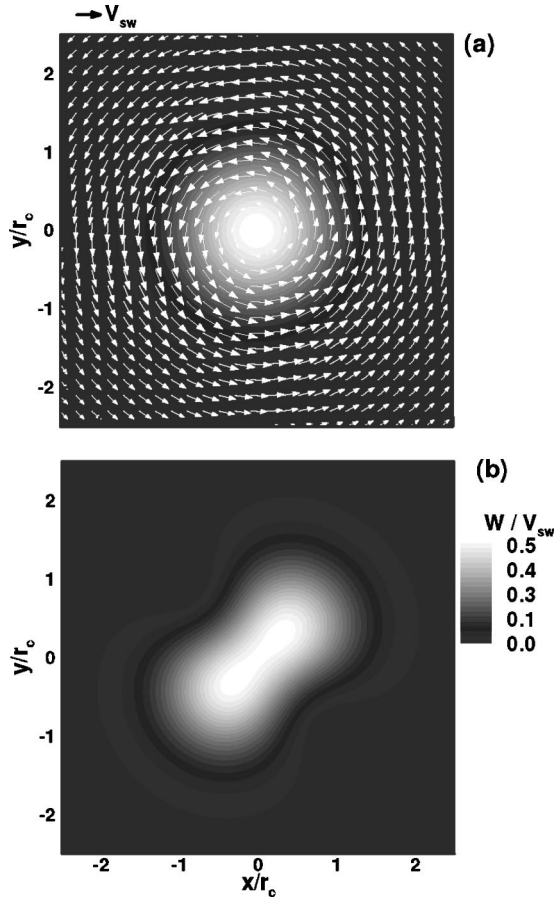

FIG. 4. (a) Simulation of an Oseen vortex with a Gaussian distribution of axial flow, and (b) the expected measured axial velocity distribution considering Eq. (1). Axial flow velocity component is indicated by flooded contours. The vortex parameters, circulation Γ and core radius r_c, were taken from the $k=11.5$ (high ω_z) case.

surements. The first is caused by the uncertainty in determining the displacement of the tagged line (i.e., due to image noise, fitting procedure, etc.). This measurement error was estimated by investigating the regions in the flow where no axial flow was expected, e.g., away from the vortex core near the freestream. The phase-averaged axial velocity measurement rms error was found to be 0.10 cm/s. Note that included in this uncertainty is also any possible unsteady nonzero spanwise flow that might naturally exist in the water tunnel.

The second source of error is due to nonzero flow velocities in the direction parallel to the tagged line. The error in line-tagging measurements caused by nonunidirectional flow has been discussed in Hill and Klewicki[14] and Koochesfahani *et al.*[15] This error can be estimated according to Eq. (1)

$$\frac{\Delta w}{w} = \tan\theta\left(\frac{\partial w}{\partial y}\right)\Delta t. \tag{1}$$

In this equation w is the velocity component perpendicular to the tagged line, Δw is the error in the estimated velocity, θ is the local flow angle given by $\tan(\theta)=v/w$ where v designates the velocity component parallel to the tagged line, and Δt is the delay time between the MTV image pair. In order to estimate the error, the vortical flow field investigated here was simulated by a Gaussian distribution of axial flow superposed on the flow field of an Oseen vortex. Figure 4(a) illustrates the simulated flow field, where the vortex parameters (circulation Γ, core radius r_c, maximum swirl velocity V_{sw}, and range of axial velocities) were taken from data for the highest reduced frequency k investigated here. Figure 4(b) shows the axial flow field that would be measured according to Eq. (1). In this work, the peak axial velocity is primarily discussed. Since the location of peak axial velocity was nearly coincident with the center of the vortex core, where the vertical velocity component was nominally zero, there was minimum error (zero error in the simulation) in the measurement of peak axial speed. Axial velocities at all other locations away from the center of vortex core, however, did have errors to varying degrees of up to ±0.2 cm/s for the limiting high k case considered here.

Since the flow field under investigation was periodic, phase-averaging methods could be utilized to process and present the final results. In this work 1000 velocity profiles were obtained and phase ordered with respect to the airfoil motion. A single oscillation cycle, corresponding to one vortex array period, was represented by a phase Φ varying between 0 and 1, which was divided into 64 phase bins. The velocity data within each phase bin were averaged to create the phase-averaged data presented here. A more detailed ex-

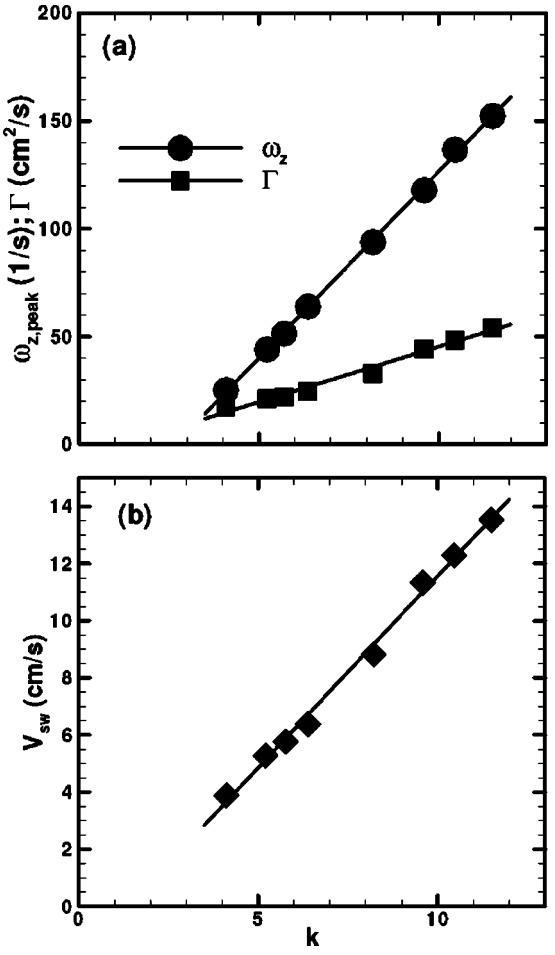

FIG. 5. (a) Peak spanwise vorticity $\omega_{z,peak}$, circulation Γ and (b) maximum azimuthal (swirl) velocity V_{sw} as a function of the reduced frequency k at $x=6$ cm. Solid lines are linear least-squares fit to data.

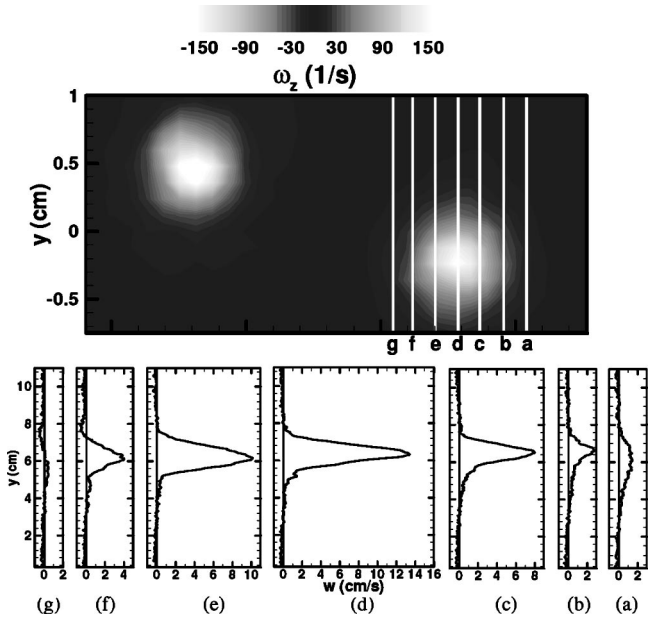

FIG. 6. Axial flow profiles for different phases relative to the vortex core location; $k=11.5$, $x=37r_c$. Vorticity contours from the midspan planar measurements are shown in the top figure.

planation of the phase averaging process can be found in Bohl.[13]

III. RESULTS AND DISCUSSION

The initially 2D characteristics of the vortex flow field were measured via two-component MTV at the center span of the tunnel using a planar MTV method; see Bohl and Koochesfahani[16] for details. These measurements provided data on the vortex parameters such as circulation Γ, peak vorticity $\omega_{z,peak}$, core radius r_c, and maximum azimuthal (swirl) velocity V_{sw}. The vortex core radius r_c was defined by the $1/e$ location for a Gaussian vorticity distribution. These data were used for correlating the axial flow information. Typical results from these measurements are illustrated in Fig. 5. The peak vorticity and the circulation of the vortices varied nominally linearly with the control parameter, the airfoil oscillation reduced frequency k. Consistent with this result, the vortex core radius r_c was found to be nearly constant at a value of about 0.41 cm throughout the range of reduced frequencies investigated here. Additionally, the vortex maximum swirl velocity V_{sw} was also found to vary nearly linearly over the reduced frequency range investigated, see Fig. 5(b). Note that the maximum swirl velocity (about 14 cm/s) exceeded the freestream speed (10.5 cm/s) at high reduced frequencies.

All the line-tagging data were acquired at a fixed spanwise location of $z=10$ cm $(24r_c)$, which was nominally half way between the tunnel side wall and midspan. The downstream measurement locations ranged between 5 cm $(12r_c)<x<45$ cm $(110r_c)$. Figure 6 illustrates a sequence of axial velocity profiles as a vortex core passed by the downstream location $x=37r_c$ for the case of the highest reduced frequency (i.e., vortex of highest circulation/vorticity) studied here. The top plot in Fig. 6 shows, for reference, the vorticity field from the planar midspan measurements.[16] Note that the location of the tagged lines was spatially fixed and the axial velocity within different parts of the vortex core was sampled as the vortex array convected past this fixed location. The measurement locations of the axial velocity relative to the vortex location are marked in Fig. 6 both by vertical lines and alphabetically. The corresponding velocity profiles from the line tagging data are indicated below. This sequence of profiles provides a clear spatial map of the structure of axial velocity. It is apparent that significant spanwise flow exists inside the core of the vortex and decreases to very low levels rapidly outside of the core. In addition to the strong axial flow within the vortex core, a weak reverse flow was also measured near the edge of the vortex core in Figs. 6(f) and 6(g). The presence of reverse flow was expected from continuity.

In the case shown in Fig. 6, a well-defined single-cell axial flow pattern was observed with a peak axial speed comparable to maximum swirl speed. The downstream evolution of axial flow profile was influenced by the vortex strength. This is illustrated in Fig. 7 by contrasting results from two cases whose peak spanwise vorticity was different by about a factor of 3. In this figure, axial velocity profiles only at the

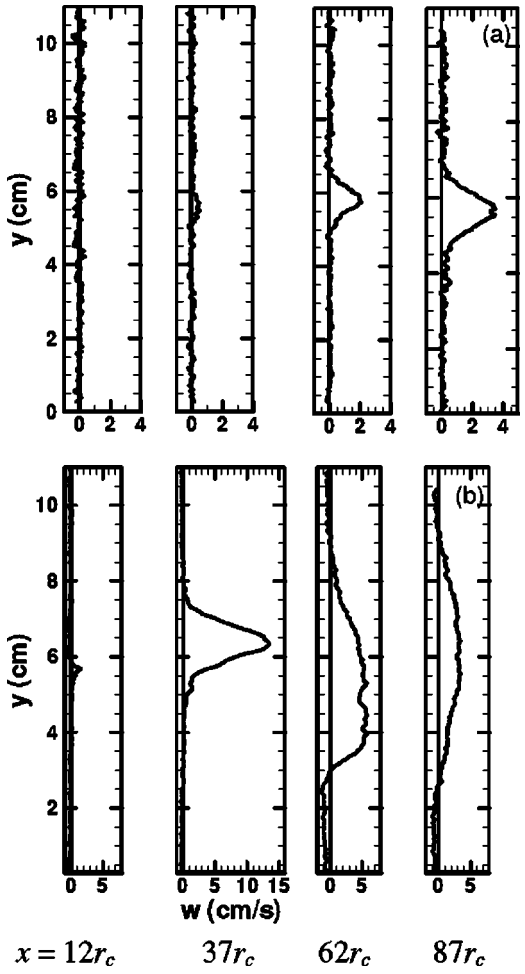

FIG. 7. Downstream progression of axial flow profiles for (a) $k=5.2$ (low ω_z) and (b) $k=11.5$ (high ω_z). Note that velocity scale is different for (a) and (b).

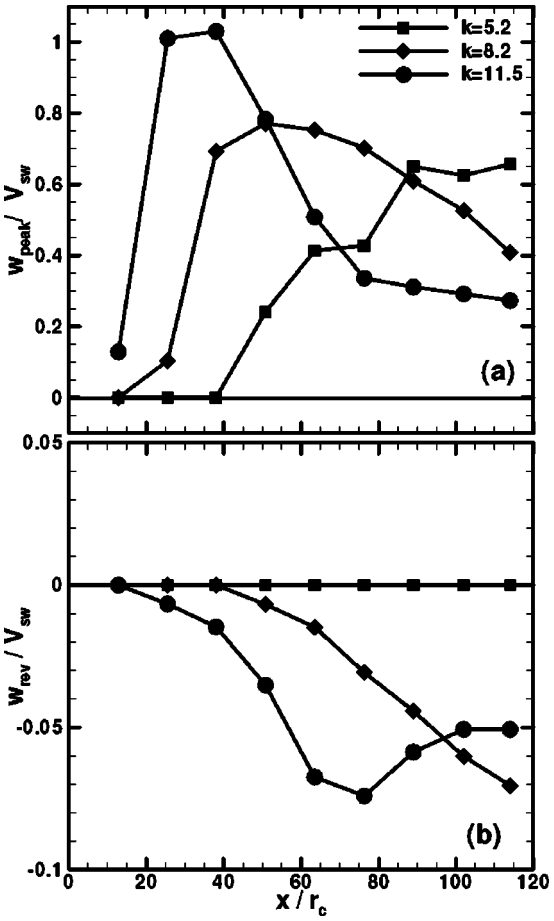

FIG. 8. (a) Peak axial velocity and (b) peak reverse axial velocity as a function of the streamwise distance.

center of the vortex core are shown at four selected downstream stations. The streamwise progression of the axial flow profile for $k=5.2$ (relatively low vorticity ω_z) is shown in Fig. 7(a). No axial flow was present at the first measurement location $x=12r_c$ (5 cm). At $x=37r_c$ (15.2 cm) there was evidence of a small bump in the profile at $y=5.5$ cm, indicating that axial flow was entering the measurement field. At $x=62r_c$ (25.4 cm) a more pronounced axial flow was measured and by $x=87r_c$ (35.7 cm) the peak axial flow speed increased by a factor of nearly 2.

The downstream progression of the axial flow profiles for $k=11.5$ (relatively high vorticity ω_z) is shown in Fig. 7(b). There was an indication that the axial flow from the vortex/side-wall interaction had already reached the line-tagging measurement location by $x=12r_c$. As the vortex convected downstream to $x=37r_c$ the axial flow increased rapidly to a significant level while maintaining a smooth, visually regular profile. At this downstream location the peak axial flow speed was nominally equal to the maximum swirl velocity. A weak reverse axial velocity (i.e., towards rather than away from the sidewalls) was also measured outside of the vortex core at this downstream location, as shown earlier in Figs. 6(f) and 6(g). The profile through the center of the vortex core [see Fig. 7(b)] did not indicate reverse flow, suggesting that the reverse flow was not symmetric about the vortex core along the x axis. Note that the axial flow in this high vorticity case evolves much more rapidly than its low vorticity counterpart shown in Fig. 7(a). By the time the vortex convected to $x=62r_c$ the nature of the axial flow profile had changed noticeably; the axial velocity had decreased significantly in magnitude, and the spatial extent over which the axial flow occurred had increased. The reverse flow, first observed at $x=37r_c$, became more pronounced at $x=62r_c$ with a value reaching nominally 18% of the peak axial flow at that downstream location. Farther downstream at $x=87r_c$ the trend of decreasing peak axial flow speed and increasing spatial extent, observed at $x=62r_c$, continued. The magnitude of the peak reverse flow speed remained nearly constant though it increased to 25% of the local peak axial flow value.

Two particular features of the axial flow profiles were selected for further scrutiny. The peak values of positive and reverse axial velocity were determined from profiles such as those in Fig. 7 at each downstream measurement location. The variation of these two features over the entire downstream distance investigated is plotted in Fig. 8 for three different levels of peak spanwise vorticity; $k=5.2$ (low ω_z), 8.2 (mid ω_z), and 11.5 (high ω_z). The general observation from this figure is that as vorticity level gets higher, the downstream evolution of axial flow occurs more rapidly. The

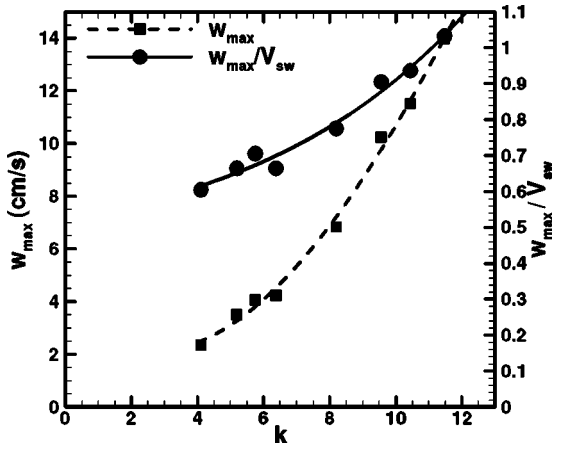

FIG. 9. Maximum positive axial velocity for all measurement locations as a function of reduced frequency k.

peak positive axial flow speed, Fig. 8(a), increased slowly in magnitude for the $k=5.2$ case as the downstream distance increased, appearing to reach a plateau for $x>87r_c$. The $k=8.2$ case showed a rapid increase in the peak positive axial flow speed for $x<50r_c$, followed by a slower decrease in the magnitude for $x>50r_c$. For $k=11.5$, the initial rate of increase of peak positive axial flow (i.e., for $x<37r_c$) was even faster than that in the $k=8.2$ case. The peak velocity then decreased rapidly in magnitude over the range $37r_c<x<75r_c$, after which the rate of decrease in the peak axial flow was reduced. The peak reverse axial velocity versus the downstream distance is shown in Fig. 8(b). The reverse flow speeds were significantly smaller than the positive axial flow. For the $k=11.5$ case, the reverse flow increased rapidly and reached a maximum near $x=75r_c$, followed by a decreased in magnitude for $x>75r_c$. Note that the downstream locations of the maximum positive and maximum negative axial flow speeds were not coincident. The $k=8.2$ case showed an initially slower rate of increase. In contrast to the $k=11.5$ case, no global maximum level was indicated for $k=8.2$ within the measurement extent. No evidence of reverse axial flow was detected, within the resolution capability of the current measurements, for the $k=5.2$ case.

To get a general quantitative sense of how the strength of the vortex influenced the axial flow magnitude, the overall maximum axial velocity over the entire streamwise measurement extent is plotted in Fig. 9 against the reduced frequency. Data are presented both in real units and in normalized form in terms of the axial speed ratio (axial speed normalized by swirl speed w_{max}/V_{sw}). The lines through the data points represent a second-order polynomial fit to data. We note that the maximum axial speeds could become very large, even faster than the vortex convection speed (in this case about 10.5 cm/s). These data also indicate that the axial flow was as strong as the in-plane velocity field of the vortex; the maximum axial speed ratio varied between 0.6 and 1 for the cases investigated. The flow visualization study of Koochesfahani[6] had previously estimated axial flow speeds in the range $0.3<w/U_c<0.6$ over the reduced frequency range of $4<k<6$, where U_c corresponds to the vortex convection speed. Using the vortex convection speed data available from planar MTV measurements at the center span,[13] the results in Fig. 9 would yield $0.25<w_{max}/U_c<0.4$ for the range of reduced frequencies considered in Koochesfahani.[6] These results are in reasonable agreement, considering the qualitative nature of the original estimates based on dye displacement information.

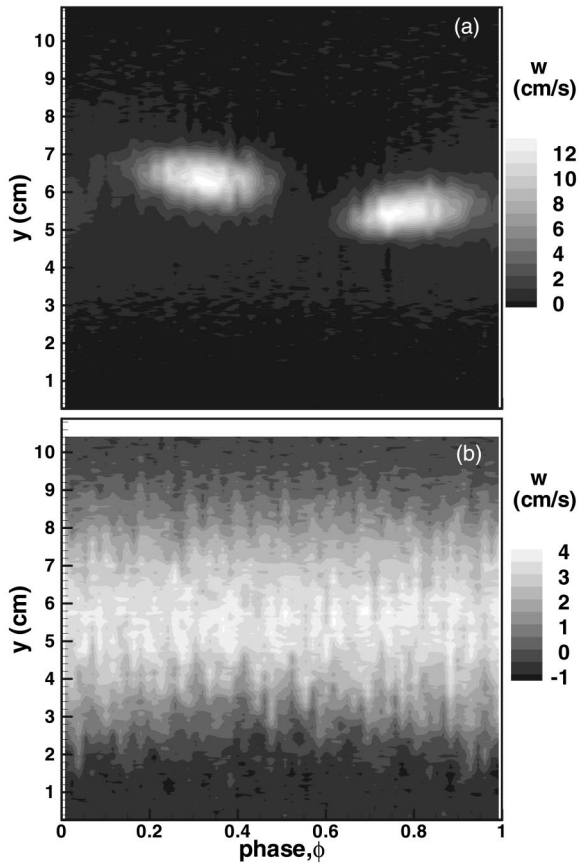

FIG. 10. Flooded contour plot of the phase-averaged axial flow velocity, w, for $k=11.5$ (high ω_z) as a function of the lateral position and the airfoil phase at (a) $x=37r_c$ and (b) $x=87r_c$.

Evidence was provided earlier in Fig. 7(b) that the nature of the axial flow profile had changed significantly with downstream distance for the case of highest reduced frequency (relatively high vorticity). We will now examine this issue in more detail. One can get a view of the overall spatial structure of the axial flow pattern at a given downstream location by plotting the phase-averaged axial velocity profiles versus phase for one complete oscillation cycle (i.e., one vortex array period). Results are shown in Fig. 10 in terms of the contour plot of axial flow at two different downstream locations for the highest reduced frequency (i.e., vortex of highest circulation/vorticity). As noted before, at the farther upstream location $x=37r_c$ the regions of axial flow were confined in two isolated structures per oscillation period. These two regions of axial flow were found to be spatially coincident with the two alternating sign vortices shed by the oscillating airfoil for each phase.[13] The oblong shape of the axial flow regions in this figure is an artifact caused by the nonzero v component of velocity around the vortex core, which adversely affects the accuracy of line-tagging data as dis-

cussed previously; see also the simulation results in Fig. 4. The interesting result was that by the time the vortices convected to the downstream location $x=87r_c$ the axial flow no longer existed in distinct isolated structures but was continuously distributed throughout the entire phase. Data, not shown here, indicated that the change in axial flow structure was also correlated with the breakup of the vortex array vorticity field from isolated structures into more widely distributed regions.[13] Dye flow visualization results of Koochesfahani[6] had also shown the downstream breakup of the vortex array, consistent with the observations here.

It would be tempting to connect the breakup effects described above to the vortex breakdown phenomenon.[17] Vortex breakdown occurs is highly swirling flows when the swirl ratio approaches unity and beyond (swirl ratio is defined to be the ratio of vortex swirl speed to axial speed, inverse of we have defined here as the axial speed ratio). In all the cases presented here the swirl ratios are certainly one or larger and we do see an increase of the vortex core diameter and significant reduction of axial flow speed. However, axial flow profiles do not reveal a reversal of axial flow within the vortex core as is often observed in vortex breakdown. Also, we see the most significant breakup effects at the highest value of axial speed ratio, or the lowest swirl ratio. A relevant effect that should also be considered is the helical instability of a vortex core when the jet-like axial speed is high enough to overcome the stabilizing effect of the swirling motion.[18] Clearly, more detailed studies are needed to understand the nature of the breakup of the vortex array and the reported fundamental change in the spatial structure of the axial flow.

IV. CONCLUSIONS

The axial flow was quantitatively measured within the cores of the concentrated vortices shed in the wake of an oscillating airfoil. The measurements were obtained using single component molecular tagging velocimetry at a fixed span location. The combination of data from the axial flow profile shapes and peak axial flow speed indicated that the structure of the axial flow evolved through three stages as the downstream distance increased. Initially, there was little or no axial flow within the vortex cores. The axial flow then entered the measurement region and it was spatially confined to isolated structures within the cores of the vortices shed by the airfoil oscillation. The maximum axial flow speed was observed during this stage and axial flow profiles appeared to be smooth functions. Farther downstream, the spatial structure of the axial flow changed to a continuous distribution of axial flow throughout the phase space. During this stage the axial flow speeds reduced significantly. The vortex strength determined how many of these three stages were observed over the fixed downstream range studied here. For the highest reduced frequency (i.e., high value of spanwise vorticity ω_z of vortex) all three stages were noted. The intermediate reduced frequency (mid ω_z) showed the first two stages over the downstream extent measured, and the low reduced frequency (low ω_z) case showed only the first stage. The maximum axial flow speed was found to be significant and varied between 60% and 100% of the maximum swirl speed of the vortices for the reduced frequencies investigated. A weak reverse axial flow was also observed, as required by conservation of mass. The cause of the reported fundamental change in the spatial structure of the axial flow at farther downstream locations is beyond the scope of this paper and requires further study.

ACKNOWLEDGMENT

This work was supported by the MRSEC Program of the National Science Foundation, Grants No. DMR-9400417 and No. DMR-9809688.

[1] A. T. Conlisk, "Modern helicopter aerodynamics," Annu. Rev. Fluid Mech. **29**, 515 (1997).
[2] T. Von Kármán, "Über laminare und turbulente Reibung," Z. Angew. Math. Mech. **1**, 233 (1921).
[3] U. T. Bödewadt, "Die Drehströmung über festem Grund," Z. Angew. Math. Mech. **20**, 241 (1940).
[4] N. Rott and W. S. Lewellen, "Boundary layers and their interactions in rotating flows," Prog. Aeronaut. Sci. **7**, 111 (1966).
[5] O. R. Burggraf, K. Stewartson, and R. Belcher, "Boundary layer induced by a potential vortex," Phys. Fluids **14**, 821 (1971).
[6] M. M. Koochesfahani, "Vortical patterns in the wake of an oscillating airfoil," AIAA J. **27**, 1200 (1989).
[7] R. Cohn and M. M. Koochesfahani, "Effect of boundary conditions on axial flow in a concentrated vortex core," Phys. Fluids A **5**, 280 (1993).
[8] J. Hagen and M. Kurosaka, "Corewise transport in hairpin vortices—The tornado effect," Phys. Fluids A **5**, 3167 (1993).
[9] T. S. Laursen, J. J. Rasmussen, B. Stenum, and E. N. Snezhkin, "Formation of a 2D vortex pair and its 3D breakup: An experimental study," Exp. Fluids **23**, 29 (1997).
[10] A. Hirsa, J. M. Lopez, and S. Kim, "Evolution of initially columnar vortex terminating normal to a no-slip wall," Exp. Fluids **29**, 309 (2000).
[11] C. P. Gendrich, M. M. Koochesfahani, and D. G. Nocera, "Molecular tagging velocimetry and other novel applications of a new phosphorescent supramolecule," Exp. Fluids **23**, 361 (1997).
[12] M. M. Koochesfahani, "Molecular tagging velocimetry (MTV): Progress and applications," AIAA Pap. 99–3786 (1999).
[13] D. G. Bohl, "Experimental study of the 2D and 3D structure of a concentrated line vortex array," Ph.D. dissertation, Michigan State University, 2002.
[14] R. B. Hill and J. C. Klewicki, "Data reduction methods for flow tagging velocity measurements," Exp. Fluids **20**, 142 (1996).
[15] M. M. Koochesfahani, R. K. Cohn, C. P. Gendrich, and D. G. Nocera, "Molecular tagging diagnostics for the study of kinematics and mixing in liquid phase flows," *Proceeding of the Eighth International Symposium on Applications of Laser Techniques in Fluid Mechanics, July 8–11, 1996, Lisbon, Portugal*, Vol. I, pp. 1.2.1–1.2.12; also in *Developments in Laser Techniques and Fluid Mechanics*, edited by R. J. Adrian, D. F. G. Durao, F. Durst, M. Maeda, and J. Whitelaw (Springer, Berlin, 1997), Chap. 2, Sec. 1, p. 125.
[16] D. G. Bohl and M. M. Koochesfahani, "MTV measurements of the flow structure downstream of an oscillating airfoil," AIAA Pap. 2003–4017 (2003).
[17] M. G. Hall, "Vortex breakdown," Annu. Rev. Fluid Mech. **4**, 195 (1972)
[18] T. S. Lundgren and W. T. Ashurst, "Area-varying waves on curved vortex tubes with applications to vortex breakdown," J. Fluid Mech. **200**, 283 (1989).